J Mater Sci: Mater Med (2007) 18:483–492
DOI 10.1007/s10856-007-2008-y

Cross-section transmission electron microscopy characterization of the near-surface structure of medical Nitinol superelastic tubing

Pavel L. Potapov · Wim Tirry · Dominique Schryvers · Valerie G. M. Sivel · Meng-Yue Wu · Dimitri Aslanidis · Henny Zandbergen

Received: 19 April 2005 / Accepted: 24 October 2005
© Springer Science + Business Media, LLC 2007

Abstract The application of Nitinol in a wide variety of medical implants is progressively increasing because of its unique mechanical properties, durability and biocompatibility. However, as Nitinol consists of about 50 at.% of toxic Ni, certain applications are still hindered by the concern of free Ni release in the surrounding tissue. The latter is controlled by the structure of near-surface layers and can be strongly affected by various surface treatments. A proper application of advanced cross-section sample preparation techniques allows us to characterize the Nitinol near-surface structure down to the nanoscale by means of transmission electron microscopy (TEM). Elemental maps of the Ti, O and Ni distribution, concentration profiles, quantification of composition as well as atomic resolution images at the surface of a Nitinol tubing are presented and the results obtained with different sample preparation and analytical characterization techniques are compared. In addition to a strong decrease of Ni towards the surface of the oxide layer and a Ti depleted layer underneath the oxide, also a possible transformation from TiO to TiO_2 is documented.

1 Introduction

Metallic materials implanted in human tissues are involved in complex electro-bio-chemical reactions including ion interchange at the implant-tissue interfaces. Among others, Nitinol implants are recognized as having unique mechanical properties—such as superelasticity, shape memory and excellent fatigue resistance [1–4]. Peripheral cardiologic stents made of Nitinol can stand more than 400 M cycles in various bending, rotary and tension-compression fatigue modes. However, Nitinol consists of about 50 at.% Ni (balance Ti), which is known to provoke severe toxicological and allergic responses. Despite a potential Ni hazard, good biocompatibility is documented [1–4] because any release of Ni is efficiently blocked by a thin titanium oxide layer formed naturally or artificially at the surface of Nitinol medical products [2, 4]. The structure of this layer is crucial for controlling biocompatibility and can be affected by various methods of surface modification such as electropolishing and passivation [1–7].

The surface structure and composition of Nitinol medical implants are commonly examined by Scanning Electron Microscopy (SEM) [5, 7–9], X-ray diffraction [7] and photoemission spectroscopy (XPS) [2, 4, 7, 11] or Auger spectroscopy [9]. These methods provide a planar view of the surface while the structure and composition might change rapidly with increasing depth. Unfortunately, information about the depth dependence available from the XPS, Auger and SEM data is of an indirect nature. A direct examination would require a cross-sectional view in the direction perpendicular to the surface and only few examples of SEM studies made on cross-sections of Nitinol can be found in the literature [8, 9]. Moreover, the spatial resolution of SEM is in many cases not sufficient to resolve possible changes in the nanoregion underneath the tube surface. As important structural and compositional changes can occur within this nanometer scale, microscopy and analytic methods with higher spatial resolution are required.

Pavel L. Potapov · Wim Tirry · Dominique Schryvers (✉)
EMAT, University of Antwerp, Groenenborgerlaan 171,
2020 Antwerp, Belgium

Valerie G. M. Sivel · Meng-Yue Wu · Henny Zandbergen
National Centre for HRTEM, TU Delft, Rotterdamseweg 137,
2628 Delft, The Netherlands

Dimitri Aslanidis
@ medical technologies N. V., Daelemveld 1113,
3540 Herk-de-Stad, Belgium

In the present article the near-surface structure of a superelastic tubing with 1 mm (outer) diameter of medical 50.9at.%Ni-49.1 at.%Ti Nitinol is characterized by advanced transmission electron microscopy (TEM) tools supported by novel sample preparation techniques. The surface of the tubing received a finishing treatment of mechanical polishing, which is the normal preparation for manufacturing peripheral stents. No further heat treatment or deliberate oxidation was performed. The present combination of TEM methods enables us to examine the structural evolution within the first 300–500 nanometer near the free surface of such a tube. The crystal structure, interfaces, grain morphology and the distribution and bonding of chemical elements can be characterized with a spatial resolution better than 1 nm. It is particularly this lateral resolution, which provides the extra benefits over other complimentary techniques and in the present paper extra attention is attributed to those aspects of the sample preparation and characterization techniques that are relevant to this lateral resolution.

2 Sample preparation for TEM

Conventionally, metallic samples for TEM are prepared by electropolishing of thin cuts from the bulk metal. Electropolishing is executed until the sample is perforated and the wedges near the perforation become transparent for TEM. This technique is, however, not useful for characterization of near surface regions because the location of perforation cannot be controlled and, in practice, never appears in the vicinity of the free surface. Thus, in the present work, we employed other thinning techniques developed originally for semiconductor and ceramic materials.

2.1 Ion milling (IM)

In this method, three cuts perpendicular to the long axis of the Nitinol tube and yielding two rings of 0.5 mm width are made using a diamond wire saw (Fig. 1a) making sure that the free surface layer is not damaged. These cuts are then glued together with their free surfaces facing each other (Fig. 1b) and mounted on a support. The whole assembly is then mechanically thinned down to a thickness of 20 μm (Fig. 1c) followed by Ar^+ ion milling from both sides in the vicinity of the junction plane until perforation occurs (Fig. 1d). Usually, at least one of the surface layers appears to be TEM transparent.

During ion milling, the incidence angle of the ion beams is kept between 5°–8° while the acceleration voltage is gradually reduced from 5 kV in the beginning to 1 kV at the end of the process. Under these conditions, the resulting TEM cross-sections represent adequately the intrinsic structure of the sample while the ion-induced damage is minimized. The whole process might take from several hours to several days and the final thickness of the thinned region of the sample is between 20–40 nm.

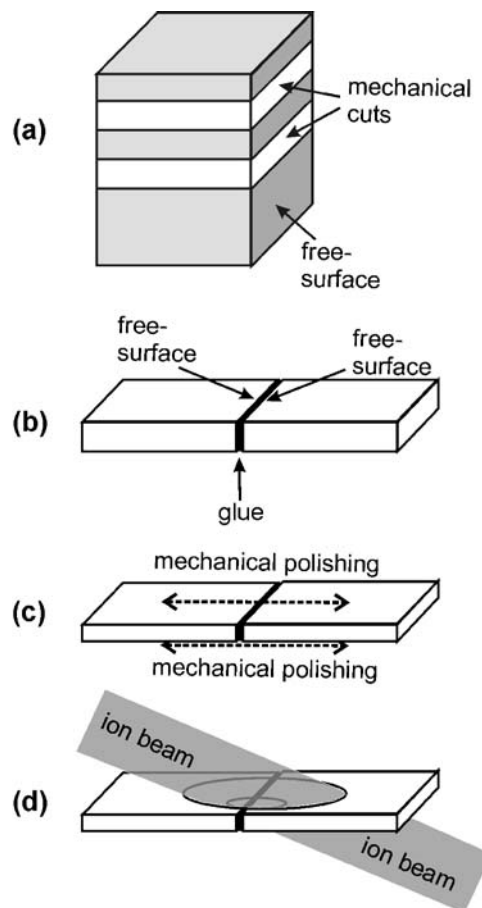

Fig. 1 Schematic sequence of the ion milling process for sample preparation for TEM.

Still, the location of perforation cannot be controlled very precisely, thus the geometry of the resulted TEM samples might vary significantly. The fraction of failures (i.e. the absence of electron transparency in the desired region) in the ion mill sample preparation is about 50%.

2.2 Focused ion beam (FIB)

A Dual beam FIB/SEM is a combination of a focused Ga ion beam (FIB) accelerated by 30 kV with a field emission electron beam in a scanning electron microscope (SEM) instrument. Both beams focus at the same point of the sample with a probe diameter smaller than 10 nm. Trenches of controlled depth are milled by the ion beam at precisely chosen positions and imaged without any damage by the electron beam. TEM specimens can be prepared following the so called "lift-out" method by removing material from both sides of the desired cross-section followed by continued thinning down to electron transparency using decreasing

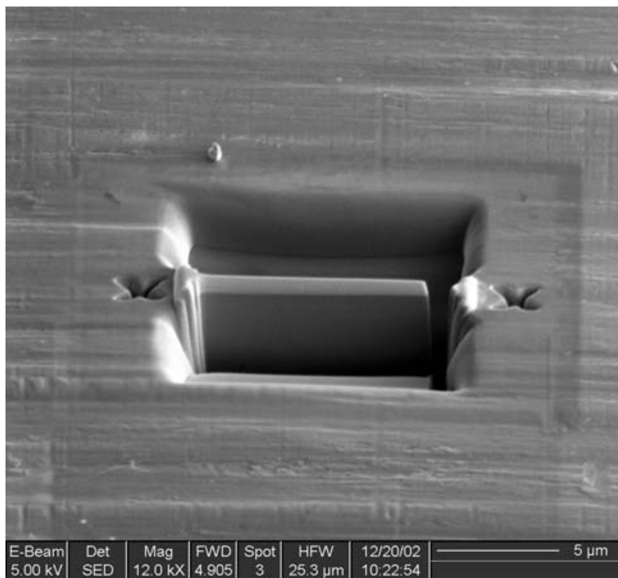

Fig. 2 TEM cross-section manufactured by FIB at the surface of a Nitinol tubing.

ion currents (Fig. 2). Finally, the produced foil is cut free and lifted out by means of the electrostatic force of a glass needle.

To prevent damaging the surface with the incident ions, the area of interest is covered in-situ with a protective platinum layer prior to FIB cutting. This Pt coating is deposited in two steps. A first thin layer is created by electron beam assisted deposition. This process is non-destructive for the surface structure. Next, a second thicker layer is deposited using the ion beam. This process is much faster but produces a defect layer due to the competition between the milling and deposition rates.

The advantage of the FIB method is that the cross-sections can be cut from any desired place at the surface of a medical product with the precision of localization of about 100 nm. The whole process takes about 2 h and produces highly reproducible cross-sections. However, the thickness of the resulted cross-sections is between 60 and 100 nm, which is noticeably higher than the typical thickness of IM samples.

For the present experiments an FEI dual beam Strata 235 FIB/SEM system was used. For regular cutting and thinning the Ga ion beam is accelerated by 30 kV while at the finishing stage of the lamella preparation the voltage was reduced to 2–5 kV.

3 Results

3.1 TEM overview

As seen in Fig. 3, both preparation methods allow us to characterize a natural oxide layer as well as a Nitinol region below the oxide. The structure of the natural oxide layer appears to be quite uniform, without visible inhomogeneities or cracks. The thickness of the oxide layer varies from 7 to 15 nm, depending on the place of examination. In the case of the ion milled samples (Fig. 3a), the free surface of the medical product, i.e. the surface normally exposed to atmosphere or tissue, is usually covered by the organic glue used in the sample preparation (see Fig. 1b). This glue layer has a clear low density and does not disturb the TEM examination of the sample. In the case of FIB samples (Fig. 3b), the sample free surface is coated by two protective Pt layers prior to FIB cutting. The first 20 nm thick Pt layer added by electron beam assisted deposition is seen as a dark amorphous layer immediately on top of the oxide. The second 600 nm thick Pt layer is deposited by an ion beam and appears in Fig. 3b as a nanograin structure with a grain size of less than 5 nm.

The bright and dark contrast features observed inside the Nitinol area in both Figs. 3a and 3b are associated with grains of 5–50 nm in size and which show different diffraction contrast due to the different crystallographic orientations of the grains under the present bright field imaging.

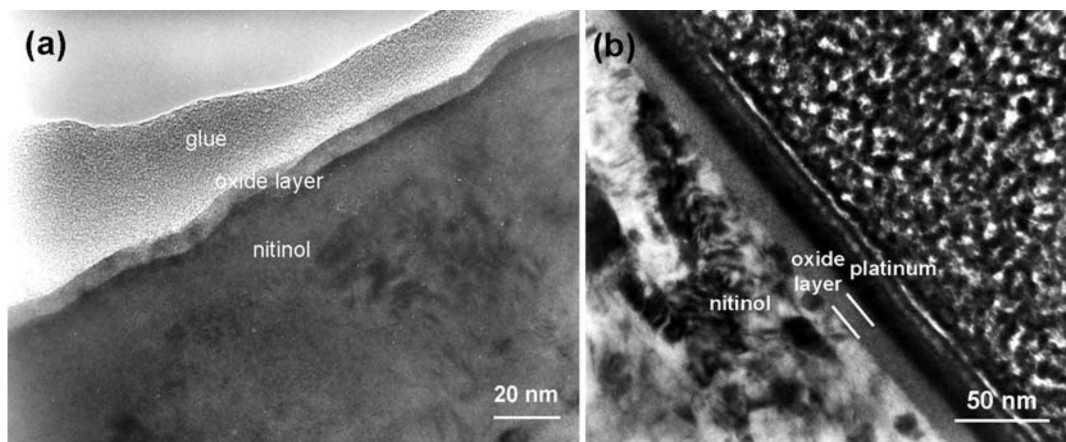

Fig. 3 TEM overview of the near-surface regions in the (a) IM sample and (b) FIB sample.

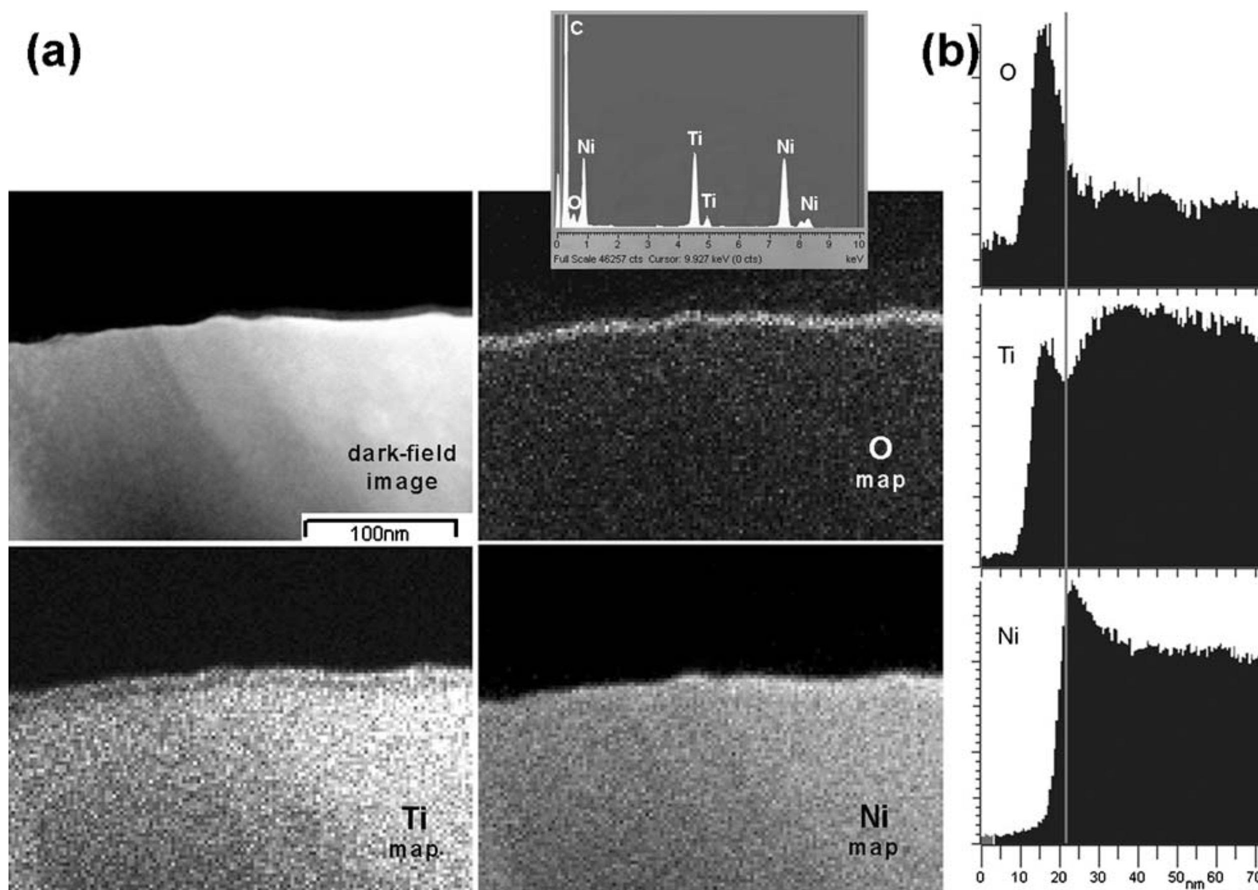

Fig. 4 STEM (a) elemental maps and (b) elemental profiles across the free surface of the IM sample obtained from the EDX spectrum (inset).

3.2 Energy dispersive X-ray spectroscopy (EDX)

The easiest way to visualize the distribution of chemical elements over the region of interest is energy dispersive X-ray spectroscopy (EDX) coupled to scanning transmission electron microscopy (STEM). The latter operates with a focused electron probe of less than 1 nm in diameter continuously scanned across the field of view. At each position, the probe generates signals captured by various detectors forming digital images. Namely, a bright-field image is formed by the detector of the transmitted beam, a dark-field image is formed by the concentric annular detector collecting diffracted beams, while elemental maps can be constructed using the EDX detector of characteristic X-ray emissions. For the present investigation a JEOL 3000F instrument was used operating at 300 kV and equipped with an Oxford INCA Energy system with a super atmospheric thin window for light element detection.

Figure 4a shows the dark field image, the total EDX spectrum (inset) and the EDX maps of an IM sample. The oxide layer is hardly visible in the dark-field image whereas it clearly shows up in the oxygen map. The Ti map reveals the metal-oxide interface, which is accompanied by a slight Ti depletion in the adjacent bulk alloy underneath.

Instead of 2D scanning, the probe also can be scanned in one direction, drastically increasing the statistics of the EDX signal. Fig. 4b shows the O, Ti and Ni elemental profiles across the surface of the IM sample: the edge or surface of the sample is located at the 10 nm measure and the metal-oxide interface is denoted by the vertical line. The drop of Ti content at the metal-oxide interface is now visualized much more clearly and can be estimated to be around 20% of the bulk Ti content. Additionally, the line scan reveals that the Ni concentration increases near the metal-oxide interface and then rapidly drops down in the oxide layer reaching its detection limit about halfway that layer.

The O, Ti and Ni elemental maps and profiles of a FIB sample are shown in Fig. 5 and resemble closely those of the IM samples (the edge of the sample is now located at the 30 nm measure). However, the disadvantage of FIB samples compared to IM ones is their larger thickness which leads to a degradation of the spatial resolution as is particularly seen from the comparison of the O maps in Figs. 4a and 5a.

Quantitative analysis of the Nitinol area in a square of 100×100 nm in the bulk alloy near the oxide layer, i.e. including the entire Ti depleted zone plus an important part of the unaffected bulk, results in a composition of 56 at.%Ni-44 at.%Ti. Taking into account that the nominal

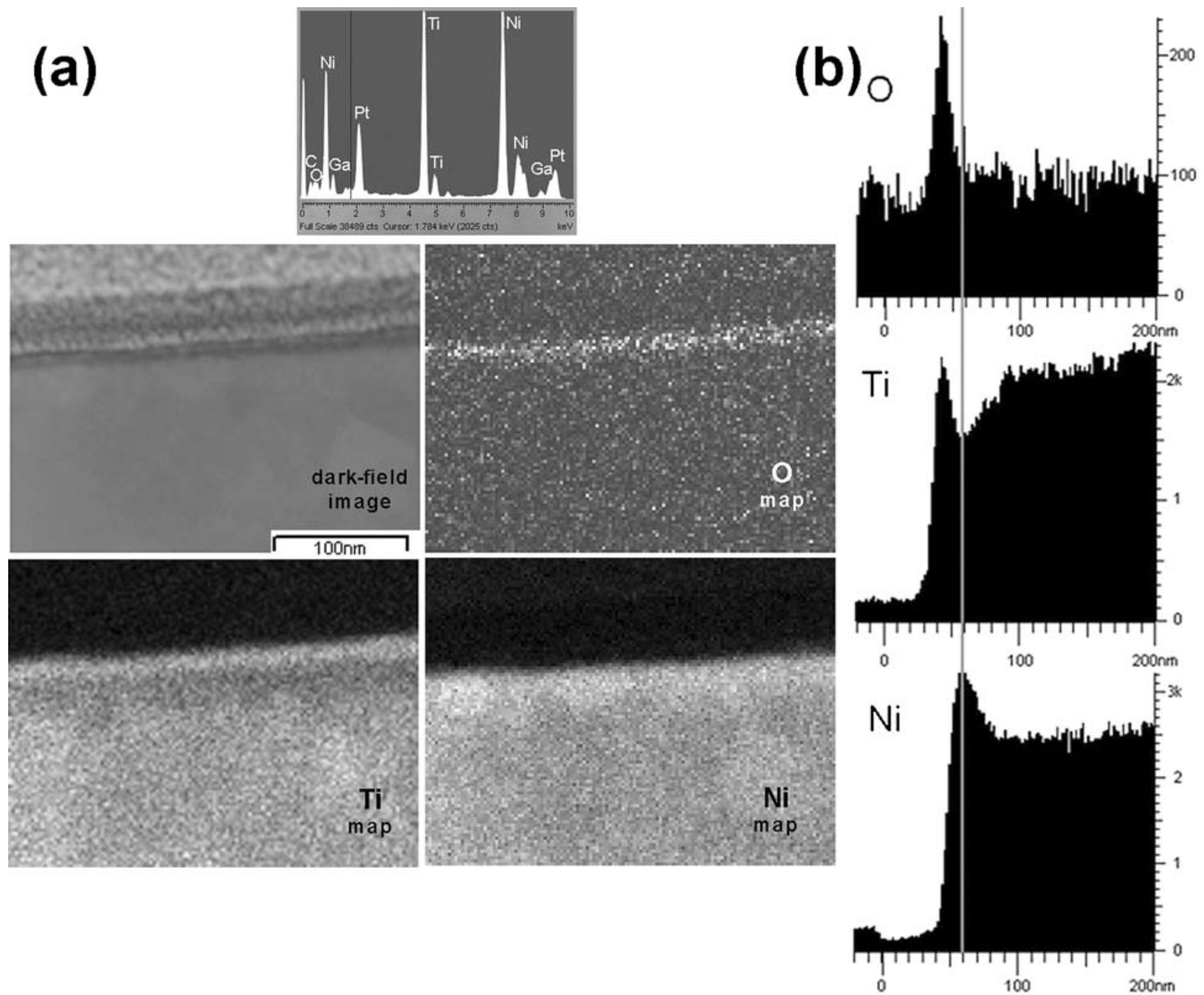

Fig. 5 STEM (a) elemental maps and (b) elemental profiles across the free surface of the FIB sample obtained from the EDX spectrum (inset).

bulk composition is 50.9 at.%Ni-49.1 at.%Ti, this result confirms the depletion of Ti near the metal-oxide interface. The composition of the oxide layer was measured as 39 at.%Ti-29 at.%Ni-32 at.%O, which indicates that this layer is dominantly titanium-oxide. However, it should be mentioned that at least part of the nickel EDX signal could be spurious, i.e. coming from the neighboring Nitinol area due to the spread of the electron beam in the sample and the possibility of multiple interaction events. In section 3.3.1 it will be shown that the real nickel content in the oxide layer is much lower than that determined by EDX.

3.3 Electron energy-loss spectroscopy (EELS)

EDX is easy in operation and processing and allows one to quantify the content of heavy elements with good precision. At the same time, however, quantification of light elements like oxygen is much less reliable because their characteristic X-ray emission lines often overlap and tend to be absorbed predominantly in the material. In contrast, electron energy-loss spectroscopy (EELS) is well suited for analyzing light elements while it also shows a higher spatial resolution due to the forward scattering of the used electrons. The latter feature also implies that the occurrence of Ni in the surface layer can now properly be examined.

EELS considers the transmitted electrons that lost energy due to inelastic interaction with a sample. An EELS spectrometer equipped with an energy filter allows one to separate electrons of different energies by using a magnetic prism. The fastest way to obtain an EELS elemental map of a given element is the energy-filtered TEM (EFTEM), in which a TEM image is formed by inelastic electrons selected in the energy range of the corresponding ionization edge. For extrapolation and subtraction of the background scattering, some extra images should be taken in the energy regions preceding the ionization edge [12]. A resolution better than 1 nm can be routinely obtained for elements having characteristic

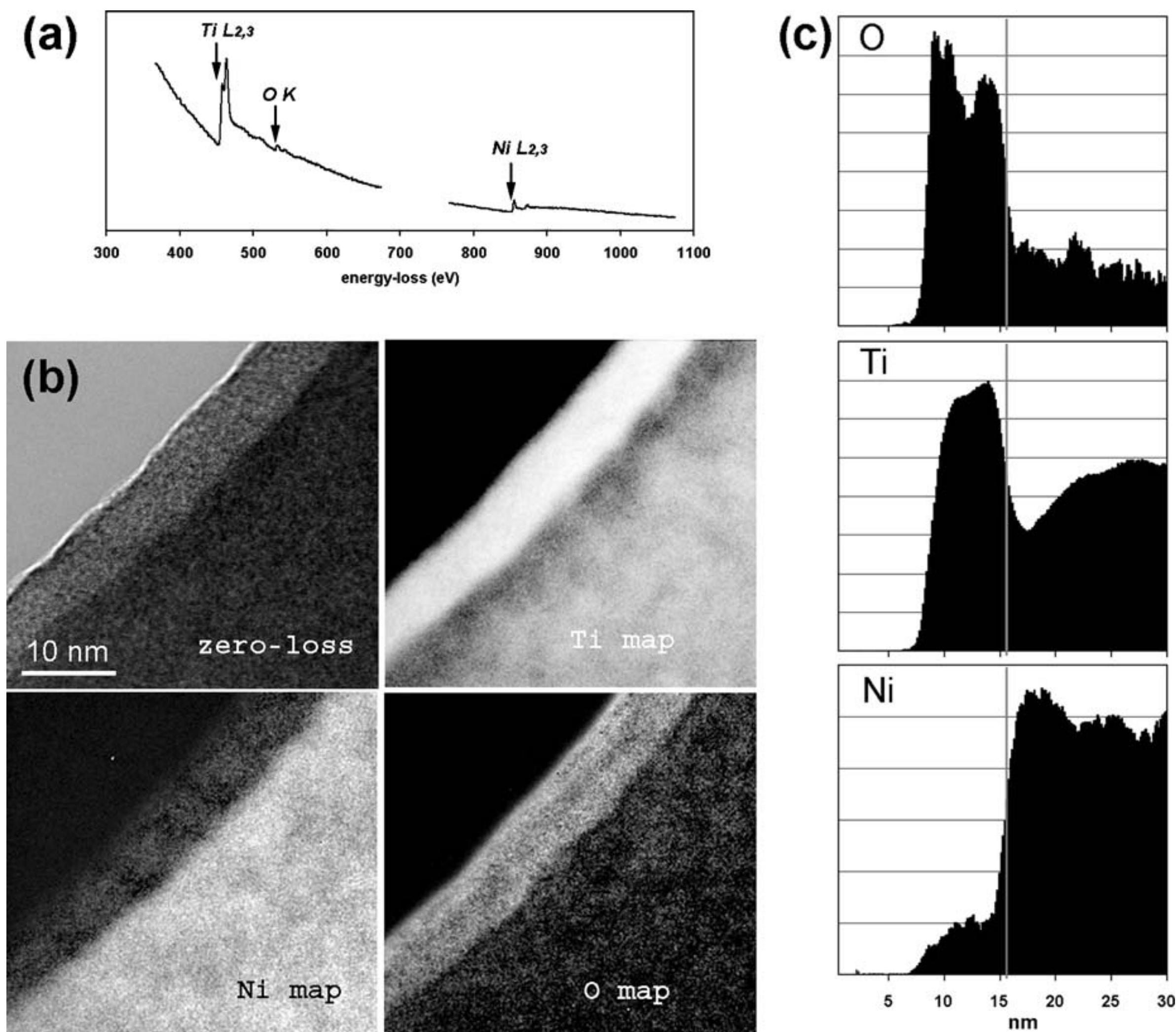

Fig. 6 (a) Typical EELS spectrum and (b) elemental maps obtained by EELS/EFTEM imaging in the IM sample. The image recorded by using zero-loss electrons is not element-specific and resembles conventional TEM images. Integration of the elemental maps along lines parallel to the metal-oxide interface resulting in (c) EELS/EFTEM elemental profiles.

ionization edges at energies less than 1000 eV, a range including oxygen, nickel and titanium.

3.3.1 EELS/EFTEM

As seen from Fig. 6a, the EELS spectrum collected near a free surface of the IM sample shows well-resolved Ti $L_{2,3}$, Ni $L_{2,3}$ and O K ionization edges. These results were obtained in an Ultratwin CM30 FEG instrument operating at 300 kV equipped with a GIF2000 (Gatan Imaging Filter) post column detector. The EFTEM elemental maps (Fig. 6b) using these edges reveal a sharp separation of the elements at the metal-oxide interface (note the increased magnification when compared with the EDX maps). The elemental profiles across this interface (Fig. 6c) confirm an increase of Ni and a depletion of Ti near the metal-oxide interface in the matrix as observed by EDX. These profiles indeed confirm that also the spatial resolution from EELS is enhanced by at least a factor of 3 compared with the EDX mapping of the same area (e.g., increased detail in the O profile in Fig. 6c). Enhancement of resolution allows us to unmask the features invisible in EDX analysis, like the small plateau of Ni in the oxide layer, which starts around the 7 nm measure. The latter result suggests that the natural oxide layer consists of a small fraction of metallic nickel or a nickel oxide. Towards the surface the Ni content again drops below the detection limit.

Again, the larger thickness of FIB samples leads to a spreading of the electron beam in the sample and degradation of the resolution in EELS/EFTEM. Additionally, the signal-to-background ratio of EELS data decreases rapidly with thickness resulting in more noisy maps. For those reasons, we have not succeeded in obtaining accurate EELS/EFTEM data or maps of FIB samples.

Quantification of the above EFTEM data results in a composition of 60 at.%Ni-40 at.%Ti when averaged in the square 15×15 nm of the Nitinol alloy directly underneath the oxide layer, i.e. primarily consisting of the Ti depleted zone. This result is in good agreement with the EDX analysis performed over the larger area (Sect. 3.2) when taking into account the fact that the EDX measurement was performed in an area extending further down into the alloy and thus including the unaltered bulk concentrations. The average composition of the oxide layer was determined as 53%Ti-5%Ni-42%O, which reasonably agrees with the EDX data in terms of the Ti/O ratio but shows a much lower Ni content than that determined by EDX. It should be mentioned that the Ni composition is measured much more reliably by EELS/EFTEM due to the better spatial resolution and absence of spurious X-rays. Also an O content is determined more precisely by EELS/EFTEM than by EDX due to the higher EELS cross-section for oxygen.

3.3.2 EELS focused probes

In an attempt to improve the precision and to obtain better spatial localization of the EELS data an analysis with focused probes was also performed. In this method, an electron beam is focused within a disk of 5–10 nm in diameter and the complete EELS spectrum is recorded providing a large amount of counts from the small region. This was done in the same instrument as the above EFTEM work. The probes in the Nitinol area reveal a composition varying from 53 at.%Ni-47 at.%Ti to 59at.%Ni-41 at.%Ti when moving from the bulk region towards the interface with the oxide, i.e. essentially the same result as in EELS/EFTEM and EDX. However, the probes in the oxide layer reveal a composition near 31%Ti-5%Ni-64%O, i.e. a higher oxygen content compared with that measured in EELS/EFTEM. The possible reason for this discrepancy will be discussed in Sect. 4.1.

3.3.3 EELS/ELNES

EELS ionization edges usually consist of several sub-edges and peaks, which are referred to as Energy-Loss-Near-Edge-Structure (ELNES). ELNES is characteristic for each given compound and can be used for identification of unknown phases. Clearly, the energy resolution of EELS spectra should be as high as possible to perform an accurate ELNES analysis. In the present ELNES work, the Technai-200FEG microscope installed at the TU Delft, the Netherlands, and equipped with a monochromator and a dedicated high-resolution GIF was employed providing, in this case, an energy resolution of 0.15 eV at a probe size of 1 nm. A STEM mode with a 1D scanning across the surface of an IM sample was used.

Figure 7 demonstrates such a fingerprint approach for the identification of the oxide layer at the surface of a Nitinol tube. Both the profiles of Ti $L_{2,3}$ and O K edges in the oxide layer resemble closely the profiles of reference TiO spectra and clearly differ from other available reference spectra of titanium oxides [13, 14]. For illustration, the ELNES of TiO_2 rutile is shown in the same figure. As a result of the low concentration of Ni in the oxide layer, no detailed study on the structure of the Ni $L_{2,3}$ edge could be performed and thus no conclusion on the metallic or oxidic character for Ni could be obtained.

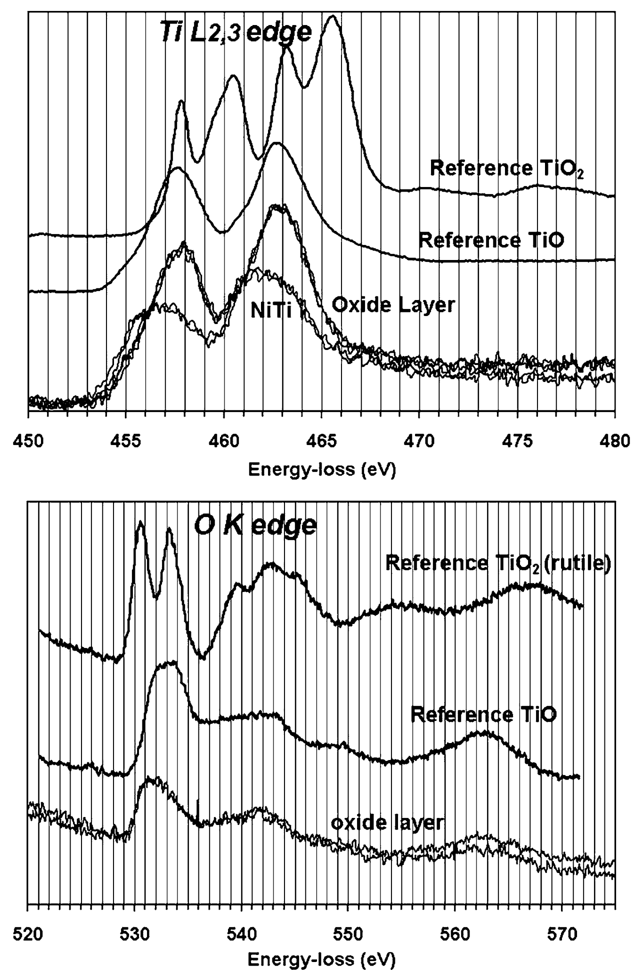

Fig. 7 High-energy-resolution EELS spectra of the Nitinol and oxide layer in comparison with reference spectra. The Ti $L_{2,3}$ and O K edges of the oxide layer fit the TiO reference.

3.4 High resolution TEM (HRTEM)

In electron microscopy, resolution of individual atomic columns is achieved by careful adjustment of various aberrations and accurate orientation of the sample along certain crystallographic orientations. Such a microscopy method is referred to as High Resolution Transmission Electron Microscopy (HRTEM) and in the present work a top-entry JEOL 4000EX with a LaB_6 filament was used. In the case of the

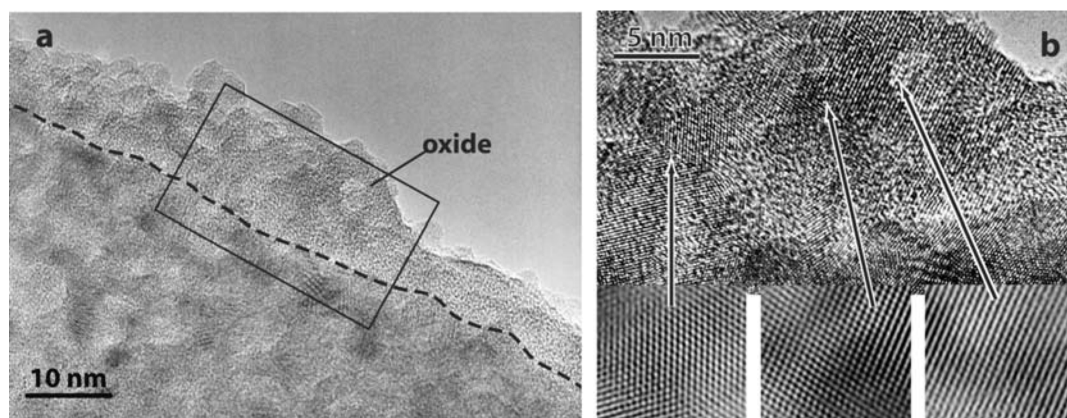

Fig. 8 (a) HRTEM image of the near-surface region in the IM sample. The dashed line marks the approximate location of the metal-oxide interface. The outlined rectangular area is zoomed in (b) and further zoomed in the insets. For better visualizing of the atomic columns, the patterns in the insets are Fourier-filtered.

near-surface structure of the medical Nitinol tubing, such an accurate orientation is not possible because of the extremely small grain size in both Nitinol and oxide layer. Nevertheless, atomic columns can be visualized in a few grains with accidentally favorable orientations and located in very thin regions of TEM samples.

Figure 8a shows the HRTEM image of the IM sample near the oxide layer. Small grains of 5–10 nm in size are seen both in the Nitinol and the oxide layer suggesting that the latter is, at least partially, crystalline. HRTEM images frequently show a symmetry lower than that expected for the cubic TiO lattice but fitting the tetragonal TiO_2 rutile or anatase structures. For instance, the atomic arrangement in the lower-left zoom in Fig. 8b can arise from the [100] orientation of TiO_2 rutile or the [331] orientation of TiO_2 anatase but is inconsistent with any orientation of the TiO lattice. Unfortunately, the small size of the observed crystalline regions excludes accurate tilting and prevents the observation of more HRTEM images from the same grain so that a clear identification of the crystal structure by HRTEM cannot be obtained.

4 Discussion

The present results clearly show that, using the above listed techniques, it is possible to obtain very detailed structural and chemical information down to the nanoscale on surface and sub-surface layers of metallic wires used in medical devices. Depending on the need for resolution, precision and accuracy cross-section IM or FIB samples can be selected and investigated by EDX or EELS in combination with HRTEM. In the present examples these combined techniques have allowed us to observe and quantify the concentration of heavy (Ni, Ti) as well as light elements (O) in an oxide surface layer of 10 nm thickness freshly formed at room temperature, detect and quantify a Ti depleted layer of 10–15 nm thickness just below the oxide layer and confirm the drastic drop in Ni content in the first half of the oxide layer (i.e., 5 nm width) ending in a plateau with around 5 at.% Ni and a further decrease below the detection limit towards the surface. The peak in the Ni concentration and the Ti depletion below the oxide layer confirm earlier results, but the extend of the Ti depletion layer, up to 20% of the bulk Ti content, is surprisingly strong for a natural oxidation at room temperature [7].

As described above, most of the analytical TEM results (EDX, EELS/EFTEM, EELS/ELNES) identified the oxide layer at the surface of Nitinol as TiO, while some results (EELS/focused probes, HRTEM) indicate the existence of TiO_2. These results are summarized in Table 1. Here it should be mentioned that EELS using focused probes as well as HRTEM methods apply a higher electron dose to the sample

Table 1 Identification of the oxide layer by different TEM methods

Method	Results	Comments	Identification of oxide layer
EELS/EFTEM	53at.%Ti-5at.%-42at.%O		TiO
EELS/ELNES	Match TiO spectra		TiO
EDX	39at.%Ti-29at.% Ni-32at.%O	At least part of Ni signal is spurious	rather TiO
EELS/focused probes	31at.%Ti-5at.%Ni-64at.%O		TiO_2
High Resolution TEM	TiO_2 rutile or anatase lattice	Accurate HR work is hampered by the small grain size	TiO_2

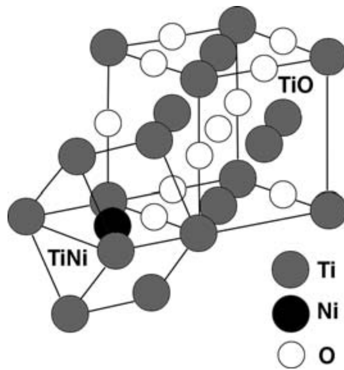

Fig. 9 Hypothetic relationship between the Nitinol and TiO lattices. The Ti-Ti distance in TiO (0.3036 nm) is close to that in Nitinol (0.3010 nm) making the $(100)_{TiO} \parallel (100)_{NiTi}$ interface energetically profitable.

and are thus more damaging when compared with other methods. Moreover, the presented results stem from a series of several experiments during which the samples were also removed from the microscope vacuum. Thus, the possibly damaged structure was unavoidably exposed to atmosphere which could lead to the formation of the more stable TiO_2.

Experimental evidence for the preferential formation of TiO at a freshly polished Nitinol surface can be understood in terms of the similarity of parts of the TiO and Nitinol lattices. TiO has a cubic lattice with a lattice parameter of 0.4293 nm while austenitic Nitinol has a cubic lattice with a lattice parameter of 0.3010 nm. Being oriented as $(100)_{TiO} \parallel (100)_{NiTi}$ and $[010]_{TiO} \parallel [011]_{NiTi}$, the Ti positions in both lattices match each other almost perfectly with only a 0.85% distortion of the Ti-Ti distance at the interface, as seen in Fig. 9. Such an interface should show a low free energy [15] and is expected to be formed more easily than interfaces with TiO_2 rutile or anatase lattices. The present observation of TiO in a freshly formed oxide at room temperature confirms the conclusions of Firstov *et al.* for samples oxidized below 500°C [7]. The present work, however, does not allow any further conclusions on the oxidation versus metallic state of the low Ni amount in the oxide layer. After a small plateau in some cases, the Ni content drops below the detection limit at the surface, contrary to the XPS observation of a 300°C oxidized sample by Firstov *et al.* [7].

As demonstrated in Sect. 3, data obtained on the IM and FIB samples correlate quite reasonably with each other. Due to the smaller thickness, the IM samples are preferable for the accurate structural characterization providing always a better spatial resolution and a higher signal-to-noise ratio than the FIB ones. Further improvement of the FIB technique reducing the thickness of TEM cross-sections is therefore desired. However, FIB could be an attractive alternative for the cases when the spatial resolution of the analysis does not need to be better than 2–3 nm, e.g. the Ti depletion as well as the Ni enrichment are both observed in the FIB and IM samples.

5 Conclusive remarks

The combination of advanced thinning techniques and analytical TEM methods allows one to visualize the nanostructural changes and distribution of chemical elements near the free surface of Nitinol medical products. In contrast to most other microscopic and analytical techniques, a cross-sectional view can be obtained.

The developed technique has been applied for the examination of a superelastic Nitinol tubing used for manufacturing peripheral cardiologic stents. It is demonstrated that

i) The thickness of the oxide layer is 7–15 nm. The natural oxide layer freshly formed at the free surface of the tubing originally appears to be TiO, but some observations indicate that this TiO has been transformed into the more stable TiO_2 during observation or manipulation of the sample.
ii) The Ni content in the oxide layer drops drastically to about 5 at.%.
iii) The Nitinol alloy is fine grained and depleted in Ti by about 20% in a region of 10–15 nm near the metal-oxide interface.

It is clear that the developed routine can be applied for evaluation of various methods of surface modification such as electropolishing and passivation of Nitinol products.

Acknowledgments Part of this work was made possible by the support of the GOA project "Characterisation of nanostructures by means of advanced electron energy spectroscopy and filtering" of the University of Antwerp and by a project of the National Science Foundation of Flanders on "Functional properties of shape memory alloys: a fundamental approach."

References

1. Y. OSHIDA and S. MIYAZAKI, *Corrosion Eng.* **40** (1991) 1009–1025.
2. S. A. SHABALOVSKAYA, *Bio-Med. Mater. Eng.* **6** (1996) 267–289.
3. J. RYHÄNEN, "Biocompatibility Evaluation of Nickel-Titanium Shape Memory Metal Alloy," Ph.D. Thesis (Oulu University, Oulu, 1999) p. 3–52.
4. S. A. SHABALOVSKAYA, *Int. Mat. Rev.* **46** (2001) 1–17.
5. R. VENUGOPALAN and C. THERANIER, in S. M. RUSSEL and A. R. PELTON (Eds), Proc. Int. Conf. Shape Memory and Superelastic Tech. Monterey (2000), p. 261–270.

6. C. THERANIER, R. VENUGOPALAN and A. R. PELTON, in “Shape memory implants” L. H. YAHIA (Ed), (Springer, Berlin, 2000), p. 35–45.
7. G. S. FIRSTOV, R. G. VITCHEV, H. KUMAR, B. BLANPAIN and J. VAN HUMBEECK, *Biomaterials* **23** (2002) 4863–4871.
8. L. ZHU, J. M. FINO and A. R. PELTON, in T. W. DUERIG, and A. R. PELTON (Eds), Proc. Int. Conf. Shape Memory and Superelastic Tech., Monterey 2003.
9. C. L. CHU, S. K. WU and Y. C. YEN, *Mat. Sci. Eng.* **A216** (1996) 193–200.
10. Y. OSHIDA, R. C. L. SACHDEVA and S. MIYAZAKI, *Biomed. Mater. Eng.* **2** (1992) 51–59.
11. S. A. SHABALOVSKAYA and J. W. ANDEREGG, *J. Vac. Sci. Technol.* **A13** (1995) 2624–2632.
12. R. F. EGERTON, “Electron Energy-Loss Spectroscopy in the Electron Microscope” (Plenum Press, New York and London, 1996)
13. B. BRYDSON, H. SAUER and W. ENGELS, in M. M. DISKO, C. C. AHN and B. FULTZ, (Eds), “Transmission Electron Energy Loss Spectroscopy in Materials Science,” (New Orlean, 1991), p. 131–154.
14. P. L. POTAPOV and D. SCHRYVERS, *Ultramicroscopy* **99** (2004) 73–85.
15. S. E. KULKOVA, (2003) private communication.